Thermomechanical Modeling of Stability of Large Low Shear Velocity Provinces

Elvira Mulyukova, Marcin Dabrowski, Trond H. Torsvik.
Physics of Geological Processes, University of Oslo, Norway

ABSTRACT

1

The thermomechanical evolution of the Earth remains a highly disputed subject. There are, however, some seemingly robust observations. A few are the focus in this study: (a) Tomographic studies, reconstruction of continental motion and rotation, and geodynamic modeling infer that the antipodally located Large Low Shear Velocity Provinces (LLSVPs) at the base of the mantle are stable, long-lived and impose the planform of flow in the mantle and of plate tectonics at the surface (Dziewonski 2010). (b) Studies of post-glacial rebound data, geoid highs and lows and geochemical mixing suggest that the average lower mantle viscosity is between one or two orders of magnitude greater than that of the upper mantle (Dziewonski 2010).
In this study, the geometry of the mantle is approximated by a hollow cylinder. The inner and outer mechanical boundary conditions are free slip and free surface, respectively. Fixed temperatures are prescribed for the thermal boundary conditions. The mantle flow is in the Stokes regime and the Boussinesq approximation applies. Newtonian rheological behavior is employed with a viscosity that depends exponentially on temperature. The large-scale heterogeneities at the base of the mantle are introduced as material of an anomalous viscosity and density.
Both structured and unstructured FEM codes are developed for solving the conservation equations of energy and momentum together with the incompressibility constraint. The advection-diffusion equation is solved in two separate steps. A FEM solver is developed to model diffusion process. A mechanical solver from MILAMIN is utilized to calculate velocities. An ODE-solver is developed to model advection.
One of the objectives in this study is to develop a robust non-diffusive advection solver. Eulerian-Lagrangian advection algorithms are conventionally used to minimize numerical diffusion. In this study, three different ode-solvers are devised and compared based on their numerical cost and the obtained accuracy.
Both structured and unstructured codes are benchmarked by reproducing critical Rayleigh number and Nusselt-Rayleigh scaling for rectangular geometry, provided by the linear stability analysis and the thermal boundary layer theory, respectively. Methods are tested based on convergence of measures, such as Nusselt number, with successive grid and time-step refinement. The convection pattern and Nusselt-Rayleigh relation are compared to results from previous numerical modeling by other authors. Analytical solutions are derived where possible and used for benchmarking.

GEOLOGY OF THE INNER EARTH

2

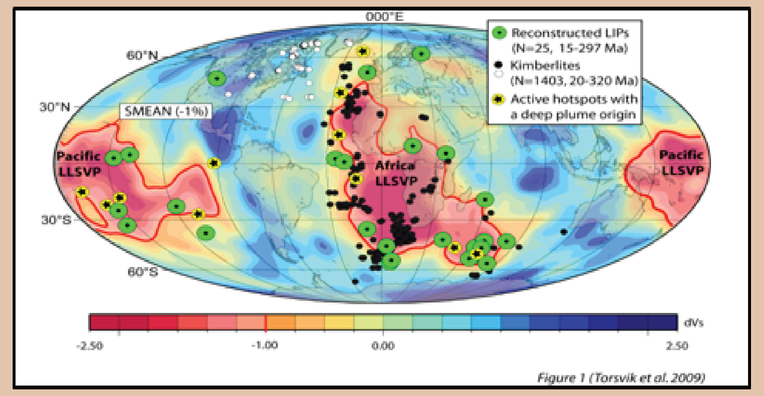

Figure 1: Reconstructed large igneous provinces, hotspots argued to have deep origin and kimberlites for the past 320 Myr with respect to shear-wave anomalies at the base of the mantle.

OBSERVATIONS

- Seismic tomography reveals two antipodally located Large Low Shear Velocity Provinces (LLSVPs) in the lower mantle, with steep margins and extending up to 1000 km from the core-mantle boundary.
- Bulk sound velocity and shear velocity within the LLSVPs are negatively correlated.
- Restored eruption sites of LIPs and hotspot volcanoes, as old as 200 Ma, project radially downwards to the margins of the LLSVPs

INTERPRETATIONS

- The LLSVPs are stable, long-lived and impose the planform of flow in the mantle.
- The seismic velocity reduction is due to thermal as well as chemical and/or phase variations, inferring that LLSVPs are comprised of material with a moderate density contrast (2-5 %).

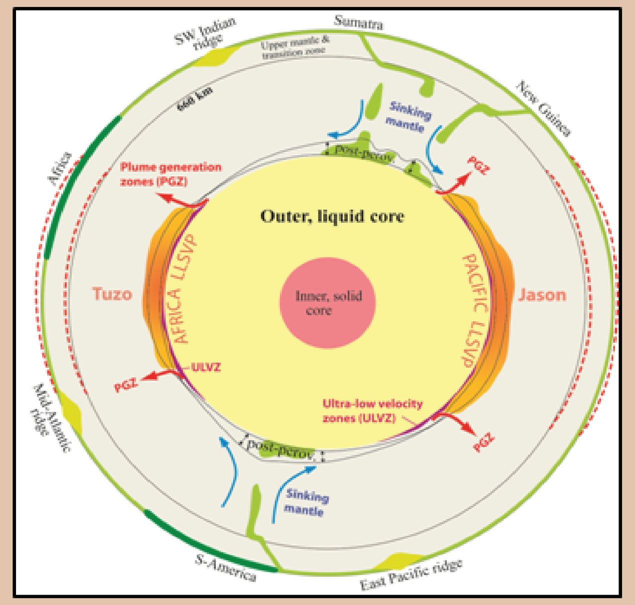

Figure 2: A cartoon of the equatorial cross-section outlining a proposed circulation in the mantle.

CONCLUSIONS

8

Using two separate grids for calculating velocities and temperatures allows having a coarser grid for the mechanical solver without significantly affecting the result.

It is advantageous to use higher-order ODE-solver schemes, such as the fourth-order Runge-Kutta, to model advection, since their computational cost is still low compared to the cost of the thermal and mechanical solvers.

Studying convergence of the Nusselt number with subsequent refining of the thermal and mechanical grids has shown significant dependence of the numerically obtained result on the grid resolution. The effect of numerical diffusion is influential on the result in a poorly refined grid. To model convection with Rayleigh number equal to 10^7 in a rectangular domain, a resolution of 400x4000 for the thermal grid is required to obtain a convergent result.

THERMOMECHANICAL CONVECTION IN A RECTANGULAR DOMAIN

6

A thermomechanical FEM code is developed to model convection in a rectangular domain. Free slip boundary conditions are applied along the four sides of the box with aspect ratio 10. Two separate grids are used to compute velocity and temperature. Results for different element sizes for both grids are presented in Figure(). The Nusselt number is calculated along the top boundary and compared to the analytical solution provided by the boundary layer theory.

RESULT FROM LINEAR STABILITY ANALYSIS:
Solving onset of convection problem for a plane layer heated from below results in analytical solution for critical Rayleigh number. For a system where both boundaries are isothermal and shear stress free, this value is

$$Ra_{cr} = 657.5$$

RESULT FROM BOUNDARY LAYER THEORY:
Considering systems with high Rayleigh numbers, changes in temperature can be restricted to the thin thermal boundary layers adjacent to the boundaries. From this, the Nusselt – Rayleigh scaling may be derived, which results in following relation

$$Nu = 1.04 * \left(\frac{Ra}{Ra_{cr}}\right)^{\frac{1}{3}}$$

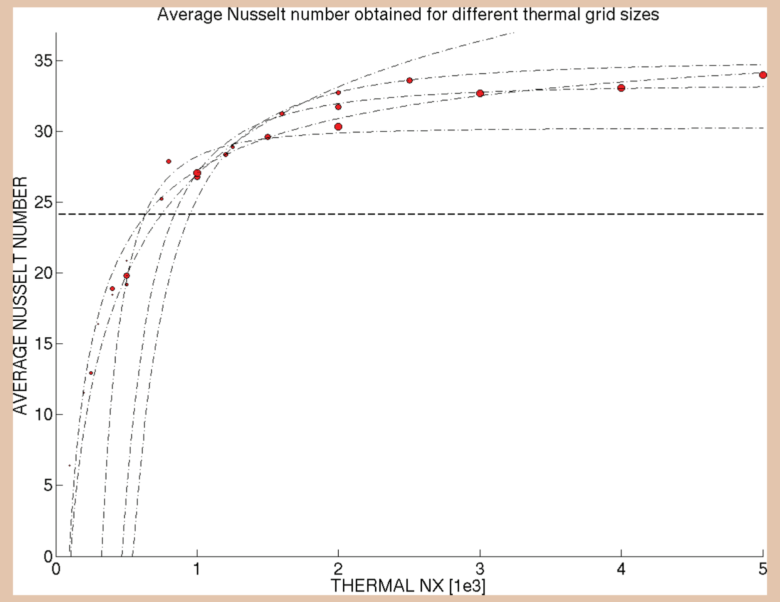

Figure 14: Time average of the Nusselt number obtained from numerical simulations with different thermal and mechanical grid resolutions. Analytical solution is plotted as a thick dashed line. Thin dashed lines are the fitted power-law functions. Total time of simulation is 3e-3* k / (c_p * rho * b^2).

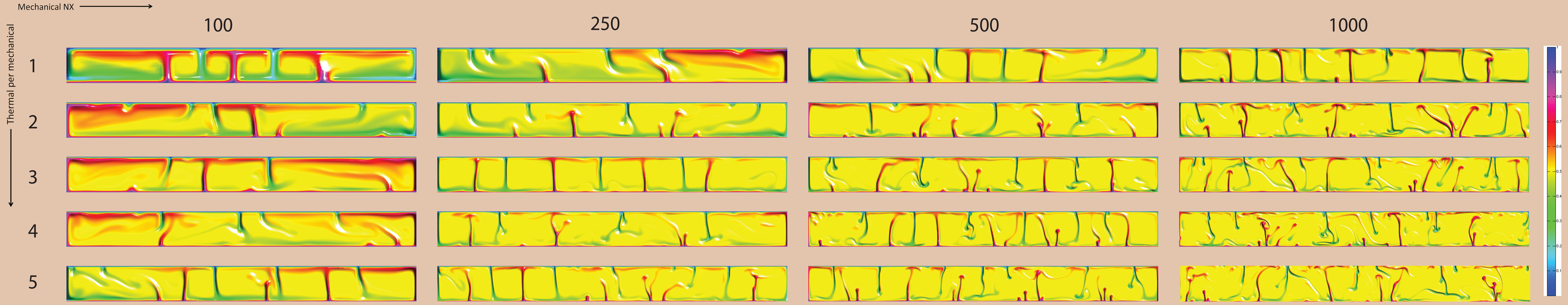

Figure 9: Patterns of thermal convection for different thermal and mechanical grid resolutions. Total time of simulation is 3e-3* k / (c_p * rho * b^2).

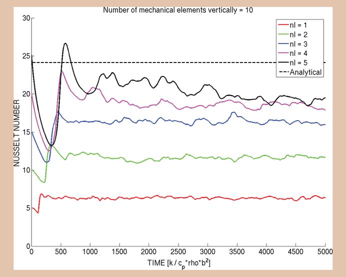

Figure 10

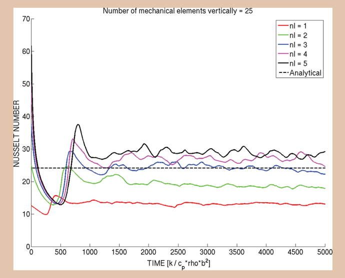

Figure 11

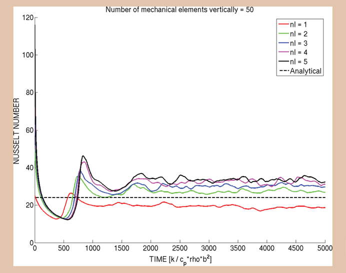

Figure 12

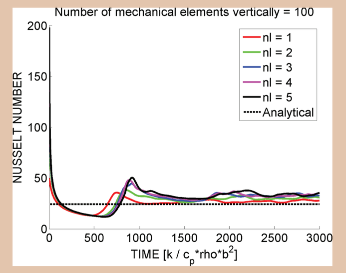

Figure 13

Figures 10-13: Nusselt number computed at the top boundary for different thermal and mechanical grid resolutions as a function of time.

PHYSICS OF THE MANTLE DYNAMICS

3

APPROXIMATIONS:

- Boussinesq approximation applies
- The flow is in Stokes Regime
- Rheological behaviour is Newtonian
- Viscosity varies exponentially with temperature

GOVERNING EQUATIONS:

Conservation of energy
$$\rho c_v \frac{DT}{Dt} = \frac{\partial}{\partial x_i}\left(k \frac{\partial T}{\partial x_i}\right)$$

Conservation of mass
$$\frac{1}{\rho}\left(\frac{D\rho}{Dt}\right) + \frac{\partial u_i}{\partial x_i} = 0$$

Conservation of momentum
$$\rho \frac{Du_i}{Dt} = -\frac{\partial p}{\partial x_i} + \frac{\partial}{\partial x_j}\left[\mu\left(\frac{\partial u_i}{\partial x_j} + \frac{\partial u_j}{\partial x_i}\right)\right] + \rho g_i$$

Viscosity-temperature dependence
$$\mu = \mu_{TOP} \cdot e^{\frac{-\theta(T - T_{TOP})}{\Delta T}}$$

GOVERNING PARAMETERS:

Rayleigh number
controls the vigor of convection

$$Ra \equiv \frac{\alpha \Delta T \rho^2 g^2 b^3 c_p}{\mu_{TOP} k}$$

Viscosity ratio

$$\theta \equiv \ln\left(\frac{\mu_{TOP}}{\mu_{BOTTOM}}\right)$$

Nusselt number
measures the efficiency of convective heat transport

$$Nu \equiv \frac{\bar{q} b}{k(T_b - T_t)}$$

THERMOMECHANICAL CONVECTION IN A HOLLOW CYLINDER DOMAIN

7

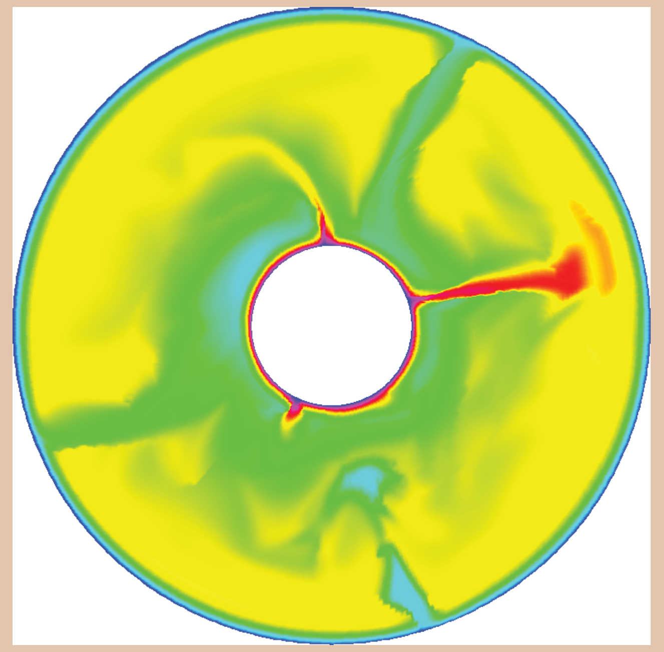

FEM DIFFUSION SOLVER

4

The conductive heat transport is modeled by solving the discretized equation of the transient heat diffusion. To do this, a FEM diffusion solver is developed. Performance of the solver is evaluated for different element types and grid resolutions. An analytical solution is found for the problem of a cooling cylinder in two dimensions, and used to estimate the error of the numerically obtained solution.

ANALYTICAL SOLUTION OF A COOLING CYLINDER:

$$T = 2\sum_{m=1}^{\infty} \frac{J_0\left(\frac{g_m}{r_b} r\right)}{g_m J_1(g_m)} e^{-k\left(\frac{g_m}{r_b}\right)^2 t}$$

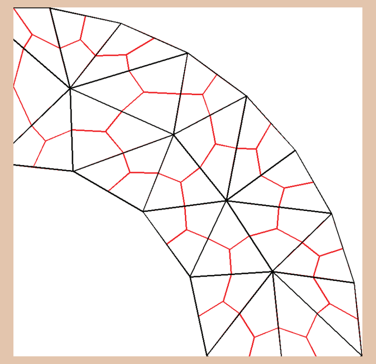

Figure 3: An unstructured triangular mesh split into quadratic elements.

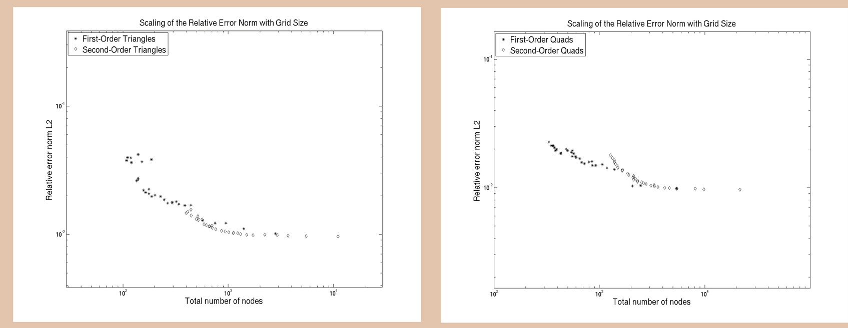

Figure 4: Scaling of the relative error norm L2 with grid size for triangular (*left*) and quadratic (*right*) elements with first- and second-order shape functions used for space-discretization.

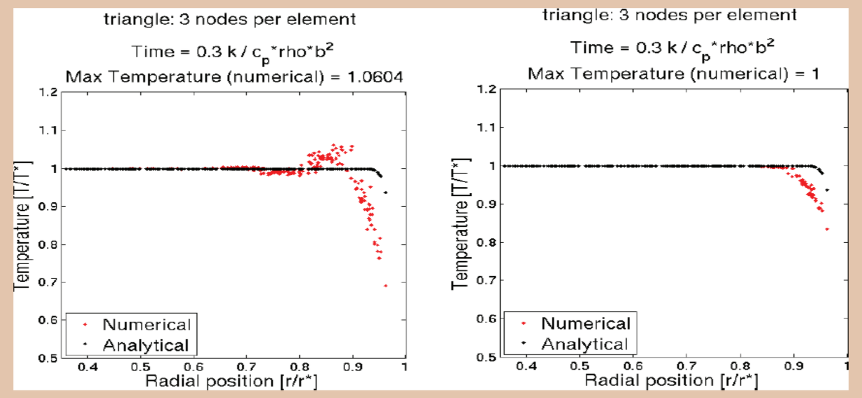

Figure 5: Analytical and numerical transient solutions to the cooling cylinder problem. First-order elements are used for the space-discretization. *Left:* Mass matrix is not lumped. *Right:* Mass matrix is lumped.

ODE SOLVERS

5

Transport of material due to convective dynamics is modeled by solving the discretized advection equation. To do this, three ordinary differential equation (ODE) solvers are developed and compared: Euler's method, fourth-order Runge-Kutta method and the embedded fifth-order Runge-Kutta method. An analytical solution is found for the problem of a passive marker advecting in a shear cell setup. The time it takes for a marker to complete a full rotation cycle and return to its original position is calculated and used to estimate the error of the numerically obtained positions.

ANALYTICAL SOLUTION OF THE TIME TO COMPLETE ONE ROTATION CYCLE:

$$I_{time} = \frac{1}{a}\int_0^1 \frac{dw}{\sqrt{(1-w^2)(1-\sin^2(ax_0)w^2)}}$$

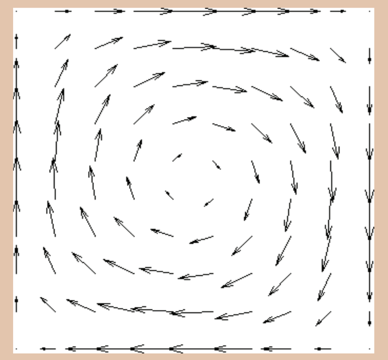

Figure 6: Stationary velocity field in a shear cell setup.

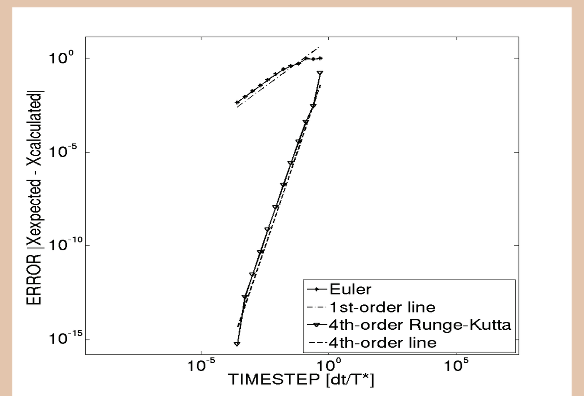

Figure 7: Scaling of error with stepsize for Euler and fourth-order Runge-Kutta methods.

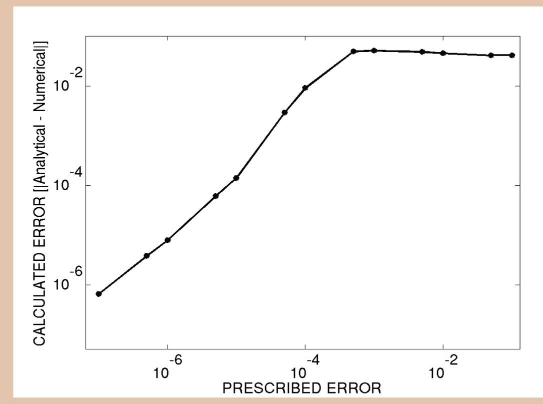

Figure 8: Correspondance between prescribed and achieved error for the embedded fifth-order Runge-Kutta method.

REFERENCES

M. Dabrowski, M. Krotkiewski, and DW Schmid. MILAMIN: MATLAB-based finite element method solver for large problems. Geochemistry Geophysics Geosystems, 9(4):Q04030, 2008.

A.M. Dziewonski, V. Lekic, and B.A. Romanowicz. Mantle Anchor Structure: An argument for bottom up tectonics. Earth and Planetary Science Letters, 299:69–79, 2010.

T.H. Torsvik, M.A. Smethurst, K. Burke, and B. Steinberger. Large igneous provinces generated from the margins of the large low-velocity provinces in the deep mantle. Geophysical Journal International, 167(3):1447–1460, 2006.